Eur. Phys. J. B **49**, 47–57 (2006)
DOI: 10.1140/epjb/e2006-00018-0

THE EUROPEAN PHYSICAL JOURNAL B

Boson peak measurements in neutron-irradiated quartz crystals

M.A. Parshin[1], C. Laermans[1,a], and V.G. Melehin[2]

[1] Department of Physics, Katholieke Universiteit Leuven, Celestijnenlaan 200D, 3001 Leuven, Belgium
[2] A.F. Ioffe Physical Technical Institute, Politechnicheskaya 26, St.-Petersburg, 194021, Russia

Received 23 September 2004 / Received in final form 11 March 2005
Published online 31 January 2006 –

Abstract. We have measured the low-frequency Raman scattering in neutron-irradiated quartz crystals with four different irradiation doses from 4.7×10^{19} n/cm^2 to 1×10^{20} n/cm^2 and for 2 different crystallographic directions. For the used doses the range of density change of the investigated samples was 12% (the maximum change during amorphization is 14%) and the amorphous fraction varied from 35% to 100%. The same measurement was done in neutron-irradiated amorphous silica with a maximal dose 2×10^{20} n/cm^2. In all cases we observed the *boson peak* in the Raman spectra. The position of the peak, at 67 ± 3 cm^{-1}, was found to be the same for all the investigated samples independent of the dose. The shape of the peak for doses 6.8×10^{19} n/cm^2 and higher was also found to be the same for 5 investigated samples (including irradiated vitreous silica). We found that the position of the boson peak in neutron-irradiated quartz crystals and vitreous silica corresponds to the Ioffe-Regel crossover frequency for phonons. The origin of the boson peak in neutron-irradiated quartz and vitreous silica can be attributed to local soft optic modes, which are analogous to the soft optic mode that drives the α–β transition in quartz.

PACS. 61.43.Fs Glasses – 63.50+x Vibrational states in disordered systems – 78.30.Ly Disordered solids

1 Introduction

The boson peak observed in the low-frequency Raman spectra of amorphous solids is a challenge for modern solid state physics. At this moment there is no common acceptable description of this phenomenon. The main question is: what kind of low-energy excitations are responsible for this peak? There are two main answers: (i) the acoustic modes due to static disorder contribute substantially to the boson peak; (ii) the low-lying local optic-like modes, which are responsible for the strong scattering of acoustic phonons at intermediate temperatures, provide a main contribution to the boson peak.

The first systematic study of low-frequency Raman scattering and infrared absorption in amorphous SiO_2, GeO_2, and B_2O_3 was presented by Stolen in 1970 [1]. The maxima in the room temperature Raman intensities were very similar to the maxima in reduced infrared absorption. The observed temperature dependence conforms to the Bose-Einstein statistics. Therefore, it was concluded that the peak in low-frequency Raman scattering and in infrared absorption arises from the same band harmonic oscillator type modes. Stolen has proposed that these modes are low-lying optical modes, which are infrared and Raman active.

Shuker and Gammon [2] have shown that in amorphous solids all harmonic vibrations can contribute to low-frequency Raman scattering, because the coherence lengths for them is short compared to the optical wavelength of laser light. This assumption leads to the breakdown of the wave-vector selection rules and the Raman-scattering intensity can be calculated from known density of states functions for each mode. For the Stokes intensity they have obtained the general expression:

$$I_{\alpha\beta,\gamma\delta}(\omega,T) = \sum_b A_b^{\alpha\beta,\gamma\delta} g_b(\omega) \frac{n(\omega,T)+1}{\omega}, \qquad (1)$$

where the summation is over all the vibration bands. Each band includes the normal vibrations, which have similar microscopic motion, frequencies, optical coupling, and correlation range. In equation (1) $g_b(\omega)$ is the density of states and $A_b^{\alpha\beta,\gamma\delta}$ the coupling constant for band b. The tensor components labeled $\alpha\beta, \gamma\delta$ are determined by the polarization of the incident and scattered light. $n(\omega,T)$ is the Bose factor at temperature T.

Martin and Brenig [3] have proposed that low-frequency Raman scattering in amorphous solids is originating from acoustic-like modes with a Debye density of states and coupling constant proportional to ω^2. In their model, the Stokes intensity is given by:

$$I(\omega,T) = A(\omega) g(\omega) \frac{n(\omega,T)+1}{\omega}. \qquad (2)$$

Also they have assumed that glasses have a continuous disordered network characterized by the correlation length. Therefore, the coupling constant was described by:

$$A(\omega) \propto \omega^2 \exp(-\omega\sigma/v)^2, \qquad (3)$$

[a] e-mail: christiane.Laermans@fys.kuleuven.ac.be

where v is the sound velocity and 2σ the structural correlation length. From equation (3) one can see that $A(\omega)$ has a maximum at $\omega \simeq v/\sigma$ and, therefore, the boson peak was interpreted as being the maximum of $A(\omega)$. This theory was widely used, because it can explain the observed frequency dependence of the Raman scattering intensity below the boson peak: $I \propto \omega^3$.

However, detailed measurements of inelastic neutron scattering [4,5] in vitreous silica in the frequency range 0.3–4 THz and with scattering vectors Q in the range 0.2–5.3 Å^{-1} have shown a large excess of additional vibrational modes in comparison with Debye density. The value of $g(\omega)$ derived from neutron scattering measurements was in agreement with the vibrational density of states obtained from the specific heat data on the same samples in assumption of a pure oxygen motion. The analysis of the observed variation of the inelastic scattering intensity with Q has shown that the contribution from sound waves is not important in the frequency range 0.3–2 THz and the dominant motion corresponds to coupled rotation of tetrahedra. It was shown also that the model, which considers the coupled rotation of five and more tetrahedra, gives a better agreement with the experimental data.

Recent hyper-Raman measurements [6] in vitreous silica have demonstrated that additional vibrational modes give the main contribution to the boson peak observed in hyper-Raman spectra and these vibrations are silent in the first-order Raman scattering due to selection rules. The important result of this work is that the boson peak in hyper-Raman scattering is shifted to lower frequencies in comparison with Raman scattering. The maximum of the boson peak was observed at 30 cm^{-1}, while in Raman scattering the maximum is at 52 cm^{-1} [1]. The position of the boson peak in hyper-Raman spectra is the same as in inelastic neutron and specific heat measurements. These results support the original idea of Shuker and Gammon [2] that the Raman intensity is given by equation (1). The coupling constant can be independent of frequency for each vibration band including the normal vibrations with similar microscopic motion. A value of the coupling constant can depend on the local symmetry of the vibrational mode.

Recent progress in inelastic X-ray scattering (IXS) with resolution of 1.5–2.5 meV allows to obtain new information about the vibrational dynamics of glasses in the boson peak region. However, interpretations of these new results are controversial [7–11]. Benassi et al. [7] have measured IXS spectra in a-SiO_2 at $T = 1050$ K and with scattering vectors Q in the range 1–6 nm^{-1}. For the interpretation of the spectra they have used a damped harmonic oscillator (DHO) model and have concluded that phonon-like propagating modes with a sound velocity of 5800 ± 200 m/s exist in the Q range 1–3.5 nm^{-1}. The linewidth of these modes is proportional to Q^2. Pilla et al. [8] have measured IXS spectra in a-SiO_2 at $T = 1200$ K at three different energy (0, 5.3 and 8.5 meV) as a function of Q in the range 2–32 nm^{-1}. They have found a Brillouin peak in the spectra at 5.3 and 8.5 meV, where energy of 5.3 meV corresponds to the boson peak energy (E_{BP}). The position of this peak shifts with increasing energy from 1.25 to 2.1 nm^{-1} that is almost proportional to the energy. It was shown that the DHO model can describe this peak rather well using $v = 6800$ m/s. The main conclusion from this study is that collective propagating excitations exist at energies above the E_{BP}.

However, IXS measurements in densified a-SiO_2 [10,11] clearly indicate the existence of the crossover from propagating to strongly scattered acoustic modes. The use of the densified a-SiO_2 have allowed to study the Q region below the expected crossover that was not possible in the mentioned above experiments [7,8]. The obtained results show that the linewidth of longitudinal acoustic waves increases very fast with frequency: $\Gamma \propto \omega^\alpha$ with $\alpha \geq 4$. The observed crossover is due to the resonance and hybridization of the sound waves with local boson peak modes. These modes are optic-like vibrations corresponding to rotations of SiO_4 tetrahedra.

New inelastic neutron scattering experiments [12] performed in vitreous silica at the same temperatures used in IXS measurements [7,8] and for the energy transfers corresponding to frequencies of 0.5, 1.3 and 2 THz have also shown the absence of the peak at $Q = 1.6$ Å^{-1} in the inelastic spectra as in the first measurements [4,5]. Simple estimates show that longitudinal and transverse sound waves in silica at the boson peak frequency of 1.3 THz have wave-vectors q of 0.13 and 0.21 Å^{-1} respectively and they must give rise to the peak at $Q = 1.6$ Å^{-1} in the inelastic spectrum, if boson peak is originated from sound waves. From the analysis of the inelastic spectra and vibrational density of states at different temperatures it was concluded that the boson peak is originated from local modes with a very small restoring force like coupled librations of SiO_4 tetrahedra.

A comprehensive study of the anomalous properties of amorphous and disordered solids leads to the conclusion that the intermediate-temperature anomalies such as the plateau in the thermal conductivity and the bump in the reduced specific heat C/T^3 are closely connected with the appearance of the boson peak in the low-frequency Raman spectra. The phenomenological soft potential model [13–17] and the microscopic elastic dipole model [18–22] successfully explain the intermediate-temperature properties by existence of quasilocal vibrations, which interact with acoustic phonons. Moreover, these vibrations and the two-level systems, responsible for the low-temperature properties, have a common origin.

According to the soft potential model [23,24] the quasilocal vibrations give the dominant contribution to the inelastic Raman (and neutron) scattering in glasses and are responsible for the boson peak. The Stokes Raman intensity is described by equation (2) with a coupling constant $A(\omega)$ independent of frequency. The boson peak appears in the reduced density of states, $g(\omega)/\omega^2$, as a result of the elastic interaction between different quasilocal vibrations. The soft potential model predicts also that the boson peak position corresponds to the Ioffe-Regel crossover frequency for acoustical phonons, which can be calculated using well known parameters of amorphous solids obtained

from low-temperature thermal and acoustical measurements. Recently, this prediction has been verified for eight glasses [25].

During the last decennary many other theories were proposed to explain the boson peak in amorphous solids. Elliott [26] has proposed that intrinsic density fluctuation domains exist in glasses. These domains cause strong Rayleigh scattering of acoustic phonons and lead to phonon localization. Therefore, a position of the boson peak is determined by the diameter of the density-fluctuation domains via the Ioffe-Regel criterion. However, the experimental study of a borate glass system [27] has shown that this model is oversimplified. The position of the boson peak is not related to the position of the first sharp diffraction peak (FSDP) in the static-structure factor. It was proposed that the type of vibrational modes and their dynamical/geometrical coupling should be taken into account. The analysis of the specific heat data in glasses with different degrees of fragility [28] has shown that the soft potential model cannot explain very low values of the excess specific heat observed in fragile glasses such as CKN, PVC, Se. It was concluded that there is no direct relation between density of two-level systems and of excess vibrations. It was also proposed that the excess specific heat is due to elastic scattering on structural fluctuations, and the observed difference in the reduced density of states, $g(\omega)/\omega^2$, is due to different amount of structural fluctuations in fragile and strong glasses. Several models [29–31] argue that the origin of the boson peak in amorphous solids is due to the force-constant disorder. Another theoretical approach in the framework of the mode-coupling theory has shown that the anomalous-oscillation peaks (AOP) produce the boson peak [32]. The AOP appear as a result of strong interaction between frozen glass structure and density fluctuations with microscopic wavelength. It was mentioned that this theory is consistent with the soft potential model. The physical model proposed by Nakayama [33] ascribes the boson peak in a-SiO_2 to localized optic-like modes with a characteristic energy and a length scale determined by density fluctuation domain due to ring size distribution. The analysis of vibrations in glasses by means of Eucledian matrix theory [34] shows that the boson peak appears due to mechanical instability transition like topological phase transition controlled by the density. Vibrations that produce the boson peak are formed by the hybridization of sound waves with high-frequency modes, which are material dependent and non-universal.

Partly disordered crystals such as quartz irradiated with fast neutrons were widely used for the study of the glassy dynamics. Low-temperature thermal and acoustic properties of the neutron-irradiated quartz crystals were found very similar to amorphous solids [35–39]. Moreover, it was shown that the disorder is created in a natural way and one can produce different degrees of disorder varying the irradiation dose. Therefore, the study of the low-frequency Raman spectra in the same samples, which were studied at low temperatures and for which tunnelling parameters are known, can help us to verify the suggested theory and to find the origin of the boson peak.

That is why we have chosen for our study neutron-irradiated quartz crystals with known tunnelling parameters. The main goal of this investigation was to study the emergence of the boson peak in neutron-irradiated quartz crystals at lower doses, than were studied previously [40,41]. At these doses the amorphous part in the sample could be relatively small and one can investigate the dependence of the boson peak position and shape on the dose.

For this purpose we have measured the low-frequency Raman spectra in neutron-irradiated quartz samples with intermediate irradiation doses between 4.7 and 9×10^{19} n/cm^2. This range was not investigated in previous works. This interval is very interesting for the study of the boson peak formation because the amorphous phase in quartz at these doses gradually grows from 35% to 90% and at a threshold irradiation of about 6×10^{19} n/cm^2 significant structural changes take place in the sample. Previous low-temperature ultrasound measurements [38], have shown that the two-level systems in the crystalline part of irradiated quartz are anisotropic. Therefore, we have studied x-cut and z-cut samples irradiated with the same doses. To make a comparison with previous works we have also measured Raman spectra of highly irradiated ($\geq 1 \times 10^{20}$ n/cm^2) and unirradiated quartz and silica.

2 Sample characterization and experimental details

Seven synthetic α-quartz samples of high purity [37], five x-cut and two z-cut, and two samples of vitreous silica, Suprasil, were shaped into a cylindrical rod with 8 mm length and 3 mm diameter. Six quartz samples and one vitreous silica sample were irradiated in the same reactor at SCK (Mol, Belgium). Use of the same irradiation conditions permits us to avoid the problems, arising when one compares irradiation doses of various reactors with quite different neutron flux distribution. The irradiation doses (for energy of neutrons above 0.3 MeV) and mass densities of the samples are given in Table 1. The mass densities of all samples were measured after irradiation by a hydrostatic method [37].

In the Table 1 one can see also the value of the amorphous fraction in the irradiated quartz samples. The amorphous fraction gradually increases from 35 to 100%. The samples N6 and N8 are quite remarkable: the N6 sample is mainly crystalline (35% of amorphous phase) and the N8 sample is mainly amorphous (70% of amorphous phase). The amorphous phase given in the Table 1 was determined as follows: for the N6 sample we used the value calculated previously in reference [37]; for sample K17 the amorphous fraction is 100%, because it is known from X-ray scattering measurements [42] that α-quartz becomes amorphous after fast neutron irradiation with dose 1×10^{20} n/cm^2; for N8 and N9 we have used a linear approximation for the calculation of the amorphous part, since the formula from

Table 1. Sample characterization: irradiation dose, mass density and amorphous phase fraction for unirradiated and neutron-irradiated quartz and vitreous silica [37].

Sample	Dose 10^{19} n/cm^2	Density g/cm^3	Amorphous phase, %
α-quartz			
unirradiated	0	2.650	0
N6	4.7	2.570	35
N8	6.8	2.395	70
N9	8.9	2.329	90
K17-Q	10	2.256	100
silica			
unirradiated	0	2.203	100
K18-G	20	2.251	100

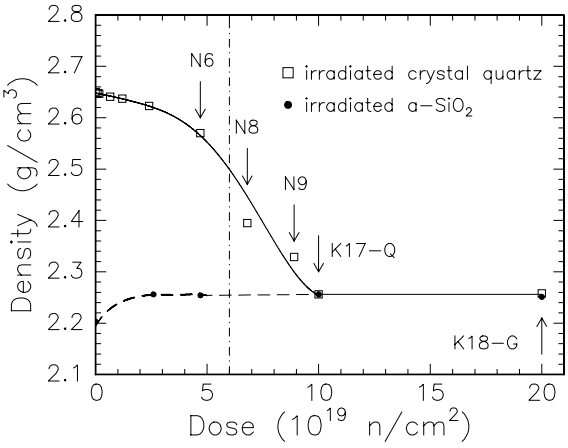

Fig. 1. Density of irradiated quartz crystal and vitreous silica as a function of the dose [37]. Arrows indicate investigated samples. The vertical dash-dotted line shows the threshold dose where significant structural changes take place in a quartz crystal [38]. The solid and dashed lines are guides to the eye only.

reference [37] is valid only for rather small concentration of amorphous regions. Our approximate values for these samples are consistent with the value 65% from reference [42] for an irradiation dose of 7×10^{19} n/cm^2 and with small-angle X-ray scattering (SAXS) measurements from reference [40], which show the presence of remnant crystallites in the sample with irradiation dose 9×10^{19} n/cm^2. From the integrated intensity of the zero-angle peak in the SAXS curve the approximate volume fraction of crystallites was found to be 7%. However, we need to mention that comparison to results of other laboratories are not readily possible due to different flux distributions in different reactors (see [43]). Here we have used for our comparison the values of the mass density as a parameter which indicates the same structural changes after irradiation. In addition we have further analyzed the behaviour of the macroscopic tunnelling parameter C for irradiated z-cut α-quartz samples (previously measured in our laboratory [44]) and have found that it repeats the linear dependence of the amorphous fraction on the dose (see Fig. 6). Since the tunnelling systems created in the crystalline part of irradiated quartz give no contribution to the tunnelling parameter in z-cut samples, one can use this parameter for the estimation of the amorphous part created in α-quartz due to irradiation. This estimate is in agreement with the used values.

The rapid decrease of the mass density ρ with irradiation dose is clearly seen in the Figure 1. Vertical arrows in the figure indicate the investigated samples. The irradiation doses for the samples N6 and N8 are close to the threshold value 6×10^{19} n/cm^2 indicated by the dash-dotted line. At this dose significant irreversible structural changes take place in quartz crystals. Crystalline quartz irradiated with a dose above this threshold evolves after heat treatment at 700–800 °C to the vitreous silica phase [45], whereas quartz irradiated with a dose below the threshold value reverts after the same heat treatment to crystalline quartz.

The Raman spectra were excited by the 488 nm line of an argon-ion laser with a power on the sample of 120 mW. Stokes and anti-Stokes spectra were recorded at room temperature in the low frequency range — from 15 cm^{-1} to 150 cm^{-1} for VV polarisation using a double monochromator Ramanor U-1000 equipped with a photon-counting system. The resolution was 2.5 cm^{-1}. The experiments were performed in the 90° geometry so that the scattered light propagated along the x-axis in the x-cut samples and along the z-axis in the z-cut samples. We have measured only polarized spectra, because the depolarization ratio is constant in this region and therefore, the position and the shape of the boson peak do not depend on the polarization (for vitreous silica a depolarization ratio of 0.30 was found in the low-frequency region $\omega < 120$ cm^{-1} [46]; and for neutron-irradiated quartz see Fig. 2 from Ref. [40]).

In the Raman spectra of irradiated quartz we observed a frequency-dependent background due to luminescence from electronic defects, which was rather high in samples N8, N9 and K17-Q. To reduce this parasitic luminescence background these samples were heat-treated for several hours at 400 °C in a hydrogen atmosphere and then measured again.

In the detailed study of the influence of heat treatment on tunnelling states in neutron-irradiated quartz [44,45] it was shown that this heat treatment does not change the tunnelling density of states $\bar{P}$ and the deformation potential γ. Raman spectra of heat-treated samples N8, N9 and K17-Q showed the absence of the frequency-dependent background. Only in the N6 sample this background is still present, but it is very small in the boson peak region in the anti-Stokes part of the spectrum. Bates et al. reference [40] have also annealed their irradiated quartz samples at 300 °C during several hours to remove the luminescence contribution.

3 Experimental results

Raman spectra (anti-Stokes part) for all x-cut investigated samples scaled and arbitrarily shifted vertically (for them not to overlap) are shown in Figure 2. In the spectra of

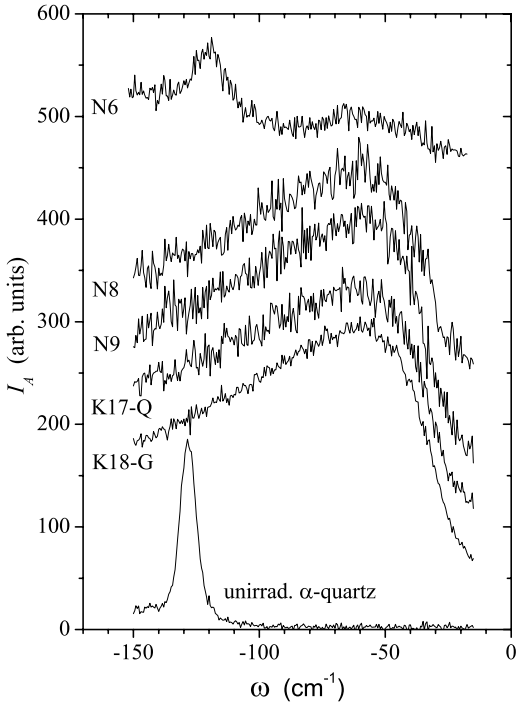

Fig. 2. Raman spectra for neutron-irradiated (N6, N8, N9, K17-Q) and unirradiated quartz (lowest curve) and neutron-irradiated vitreous silica samples (K18-G). Spectra are differently scaled and shifted vertically.

irradiated quartz crystals and vitreous silica one can see the broad peak, the boson peak, at about 65 cm^{-1}. This peak is also seen in quartz sample N6 that is mainly crystalline (65%). But in this case it is superimposed by an inhomogeneously broadened crystalline line at 128 cm^{-1}. This crystalline line is not seen explicitly in samples irradiated at higher dose, but it does not disappear at all with disorder. We will discuss in Section 4 that its presence modifies the frequency dependence above the boson peak frequency (makes it less steep).

In crystalline quartz the line was assigned to the doubly degenerated E (LO+TO) Raman line [47]. In irradiated quartz the intensity of this line is several times smaller, and it is much broader. It can be explained by inhomogeneous broadening and stress-induced splitting of the crystalline E line due to disorder induced by neutron irradiation. Stress-induced splitting of this line in crystalline quartz was investigated in details in [48]. This splitting can be seen at low temperatures, while at room temperature one observes the broad line.

We have observed also that this 128 cm^{-1} line is shifted to lower frequencies after irradiation, its maximum is at 120 cm^{-1} in quartz sample N6. The same shift was observed in a previous Raman study in a brother sample (irradiated with the same dose in the same reactor at the same time) [49]. In this study Raman spectra of five neutron-irradiated α-quartz samples (all from our laboratory except one) were measured in the frequency range 100–500 cm^{-1}. The behaviour of the four Raman lines at 466, 357, 206 and 128 cm^{-1} was studied. The obtained results have shown that in the four samples with irradiation doses $\leq 4.7 \times 10^{19}$ n/cm^2 this behaviour is similar to that observed during the α–β transition in α-quartz. In the sample with irradiation dose between our doses for N6 and N8 (it was irradiated in another reactor with dose 5.45×10^{19} n/cm^2 and the mass density of this sample was 2.46 g/cm^3) the Raman spectrum shows only one line at 466 cm^{-1}. This indicates that essential structural changes occur in α-quartz after irradiation $>5 \times 10^{19}$ n/cm^2.

As we have discussed in section 1, the intensity of the first order Raman scattering by harmonic vibrations is given by equation (2) for the Stokes Raman intensity, and by equation (4) for the anti-Stokes Raman intensity:

$$I_A(\omega, T) = A(\omega) g(\omega) \frac{n(\omega, T)}{\omega}. \tag{4}$$

As we have mentioned in Section 1, we analyse in the first approximation our Raman data in the framework of the soft potential model. According to the model, the coupling constant for light scattering from quasilocal harmonic vibrations is independent of frequency [23], $A(\omega) = A$.

The reduced Raman intensity defined as follows

$$I_{\mathrm{r}}(\omega) = A g(\omega)/\omega^2 \tag{5}$$

can be calculated from the Stokes and anti-Stokes scattering. We have compared the reduced intensity calculated from Stokes and anti-Stokes parts of the Raman spectra and indeed have found that they are the same with accuracy 3–5%. The experimental Raman intensity is proportional to this quantity at high temperatures, $kT \gg \hbar\omega$. For frequencies around the boson peak this inequality is satisfied already at room temperatures. This analysis also shows that the boson peak is not a peak in the density of vibrational states, $g(\omega)$, but a peak in the *reduced* density of states, $g(\omega)/\omega^2$.

In order to compare the shape of the spectra at different doses the reduced and scaled Raman spectra (anti-Stokes part) for the x-cut irradiated quartz crystals and irradiated amorphous silica are shown in Figure 3. One can see that the shape and the position of the boson peak (at 65 cm^{-1}) is nearly the same for the four x-cut samples with irradiation dose $\geq 6.8 \times 10^{19}$ n/cm^2. The spectrum of sample N6 has a different shape, but the position of the boson peak is also the same. In Figure 3 for comparison we show the boson peak in unirradiated vitreous silica measured on the same experimental equipment. Its maximum around 50 cm^{-1} is clearly below the maximum in our irradiated samples. The position of the maximum is in agreement with the generally known value [1,46].

We have measured Raman spectra also in z-cut samples with irradiation doses equal to the ones of N6 and N8 and found no difference compared to x-cut samples in the boson peak region (see Fig. 4). It indicates that the Raman scattering from quasilocal harmonic oscillators is isotropic.

So, quite surprisingly, starting with the dose 6.8×10^{19} n/cm^2 the position and the shape of the boson peak (at higher doses) remains nearly unchanged for all the investigated samples and does not depend on the irradiation

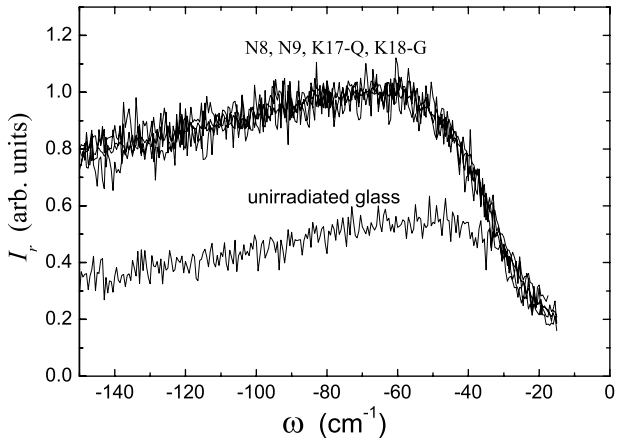

Fig. 3. Reduced and scaled Raman spectra for neutron-irradiated quartz, irradiated and unirradiated vitreous silica.

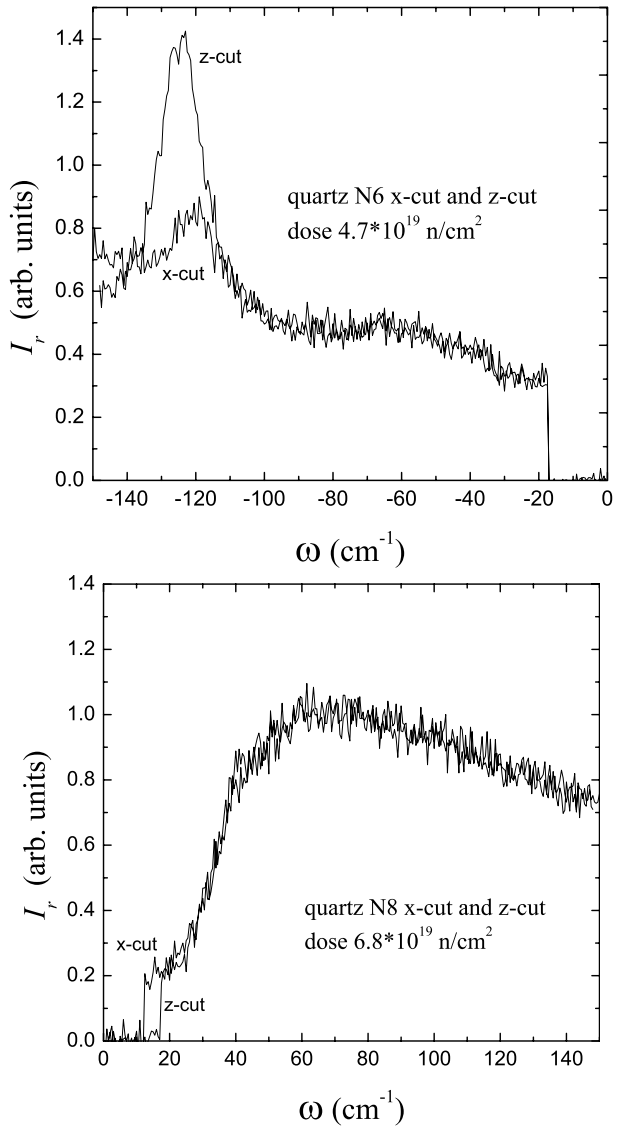

Fig. 4. Reduced Raman spectra for x-cut and z-cut neutron-irradiated quartz samples N6 and N8.

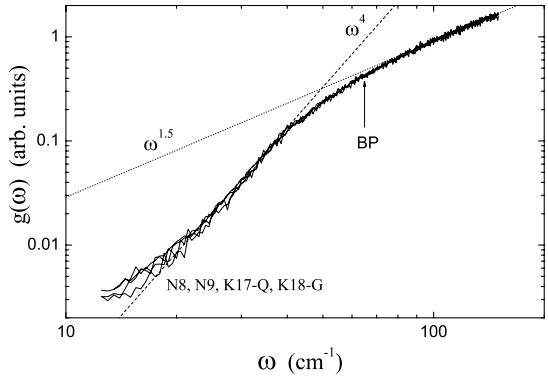

Fig. 5. Density of vibrational states (scaled) for neutron-irradiated quartz and irradiated vitreous silica (calculated from anti-Stokes Raman intensity). The arrow indicates the position of the boson peak. We assume here that the coupling constant $A(\omega)$ is independent of frequency. The dashed and dotted lines show the $\propto\omega^4$ and the $\propto\omega^{1.5}$ dependences respectively.

dose. The boson peak position in these samples is consistent with the value given by Bates et al. [40].

Measurements of Terki et al. [41] give another value for the boson peak maximum in the same quartz (K17-Q) and silica (K18-G) samples with the highest dose: 72 ± 5 cm^{-1}. This discrepancy can be explained by the fact that their samples were not annealed to remove the luminescence background from the Raman spectra. This background was subtracted artificially by means of a polynomial fit in their analysis.

4 Interpretation and discussion

As we have discussed in Section 1, the soft potential model has put forward that the quasilocal harmonic oscillators give the dominant contribution to the inelastic Raman scattering in glasses and are responsible for the boson peak. According to the model, the interaction between them leads to the very fast increase of their density of states with frequency $g(\omega) \propto \omega^4$, then the anharmonicity existing in amorphous or disordered solids stabilize the structure to a new one with the vibrational density of states $g_{new}(\omega) \propto \omega$. To verify this behaviour of the vibrational density of states in our neutron-irradiated quartz samples we have plotted in Figure 5 the value $I_{\rm r}(\omega)\omega^2 = Ag(\omega)$ versus frequency.

One can see the steep rise of the density of states below the boson peak frequency, which is indeed proportional to ω^4. Then it is changed to a more smooth dependence above the boson peak frequency. However, this dependence is a little steeper than predicted by the soft potential model: $g_{new}(\omega) \propto \omega^{1.5}$. The possible reason is that the crystalline peak observed in the samples N6 (x-cut and z-cut) at 120 cm^{-1} is very close to the boson peak position and these vibrational modes can give an additional contribution to the vibrational density of states above the peak. One can see also that for our samples there is no peak in the density of vibrational states at the boson peak frequency.

An important issue is whether the boson peak corresponds to the Ioffe-Regel criterion for acoustical phonons. In reference [23] the conjecture was put forward that the boson peak corresponds to the Ioffe-Regel criterion for phonons. At the Ioffe-Regel crossover frequency ω_d the mean free path of acoustical phonons becomes equal to the phonon wavelength $\lambda = 2\pi v/\omega_d$. Because of resonant scattering on the quasilocal harmonic oscillators the inverse mean free path of acoustical phonons has the same frequency dependence as the density of states $g(\omega)$

$$l^{-1}_{\mathrm{res,HO}} = \frac{\pi \Lambda^2}{2M\rho v^3} g(\omega) = \frac{\pi}{6\sqrt{2}} \frac{C\omega}{v} \left(\frac{\hbar\omega}{W}\right)^3 \propto \omega^4, \quad (6)$$

where M is the effective mass of a soft quasilocal vibration mode, Λ is the coupling constant describing the bilinear coupling of the soft mode with acoustical phonons, ρ is the glass density and v the sound velocity. The small dimensionless parameter C is equivalent to the macroscopic tunnelling parameter $C = \bar{P}\gamma^2/\rho v^2$ in the standard tunnelling model [50]. Here $\bar{P}$ is the density of states of the two-level systems and γ represents their coupling with phonons. The characteristic energy W in equation (6) gives the scale of levels in the soft mode. It can be determined from experimental data [14,15,17]. For example, it can be derived from the maximum in the thermal conductivity plotted as $\kappa(T)/T$ versus T: $W \approx 1.6 k_B T_{max}$, or from the minimum in the reduced specific heat $C(T)/T^3$: $W \approx 1.8 k_B T_{min}$. Usually for amorphous solids the value of W/k_B varies from 1 to 6 K [17]. For vitreous silica $W/k_B \approx 4$ K.

The scattering given by equation (6) resembles the Rayleigh scattering from glass inhomogeneities (but has a completely different origin) and is responsible for the appearance of the plateau in the thermal conductivity of glasses [16]. It was observed in vitreous silica via a non-equilibrium phonon propagation [51] and identified recently in densified vitreous SiO_2 from inelastic X-ray scattering [10]. As regards the Rayleigh scattering from glass inhomogeneities, it was shown to be too small to explain the plateau [52] and therefore can be neglected in comparison with (6). The same conclusion has been made in the elastic dipole model [18,19].

As follows from equation (6) the crossover frequency ω_d depends on two well known parameters for amorphous solids W and C

$$\hbar\omega_d \approx 0.75 W C^{-1/3}. \quad (7)$$

This conjecture was verified in reference [25]. It was found that for 8 investigated glasses the boson peak frequency ω_b (measured from Raman) is indeed proportional to the Ioffe-Regel crossover frequency ω_d for phonons

$$\omega_b \approx 1.53 \omega_d. \quad (8)$$

Therefore it gives evidence that above ω_b phonons cease to exist as well defined plane wave excitations contrary to the claims of references [7,8]. The same conclusion was made earlier from the analysis of the thermal conductivity data [53].

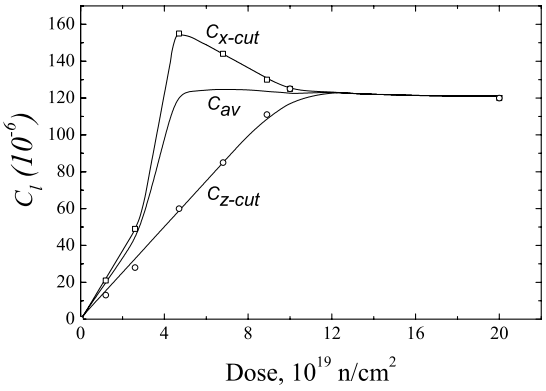

Fig. 6. Macroscopic tunnelling parameter C_l for x-cut and z-cut α-quartz samples. C_{av} is the average value $\bar{C}_l$ calculated using equation (9).

Using equations (7, 8), we calculated the boson peak frequency ω_b for our samples. According to the soft potential model $W \propto \mathcal{E}^{-1/3}$ i.e. it only weakly depends on the energy of the atomic scale $\mathcal{E}$. Therefore, it should be nearly the same for amorphous SiO_2 and irradiated quartz. For our estimates we used the same value $W/k_B = 4.2$ K as for a-SiO_2. We verified that this value is also in accordance with thermal conductivity data in neutron-irradiated quartz (with our doses), following the ideas of reference [17] where the parameters W for different amorphous solids were derived from the maximum in κ/T.

The macroscopic tunnelling parameter C_l was taken from ultrasound velocity measurements [54] for longitudinal polarization of the ultrasound. It is known that C_l from velocity measurements is more precise than from attenuation measurements. Since for different crystallographic directions of the sample it was found to be different, we used for our estimates an average value

$$\bar{C}_l = [2C_l(x-cut) + C_l(z-cut)]/3. \quad (9)$$

Using the average value of $\bar{C}_l$ for sample N6 is possible because as we will show hereafter, there is experimental evidence that the concentration of quasilocal harmonic oscillators inside the crystalline and amorphous regions are of the same order.

Indeed, as seen before from the low-temperature ultrasonic attenuation and velocity data that a substantial amount of the two-level systems resides in the crystalline part of the sample N6 and these "crystalline" two-level systems behave anisotropically [38]. To show this anisotropic behaviour we plotted in the Figure 6 the measured values of the microscopic tunnelling parameter C_l for x-cut and z-cut irradiated quartz samples. We also plotted the values of $\bar{C}_l$ calculated using equation (9). One can see that the behaviour of C_l is indeed very anisotropic for doses from 1×10^{19} n/cm^2 to 1×10^{20} n/cm^2. A remarkable observation is that $\bar{C}_l$ saturates already at a rather low dose N6 and becomes equal to that in fully amorphized quartz, although the sample N6 is still 65% crystalline. As we know the macroscopic tunnelling parameter $C_l \propto \bar{P}\gamma^2$. Ultrasound data indicate that the mean value of the coupling coefficient γ must be very similar to the value in

Table 2. Parameters C_l (Ref. [54]) and experimental and theoretical (Eqs. (7), (8)) boson peak frequencies for neutron-irradiated quartz crystals and vitreous silica samples.

Sample	C_l 10^{-6} x-cut	C_l 10^{-6} z-cut	$\bar{C}_l$ 10^{-6} average	ω_b cm^{-1} theory	ω_b cm^{-1} experim.
quartz					
N6	155	60	123	67.8	66 ± 3
N8	144	85	124	67.6	67 ± 3
N9	130	111	124	67.6	67 ± 3
K17-Q	125	125	125	67.5	67 ± 3
silica					
unirrad.	–	–	300	50	51 ± 3, 52[a]
K18-G	–	–	150	63.5	66 ± 3

[a] Reference [1].

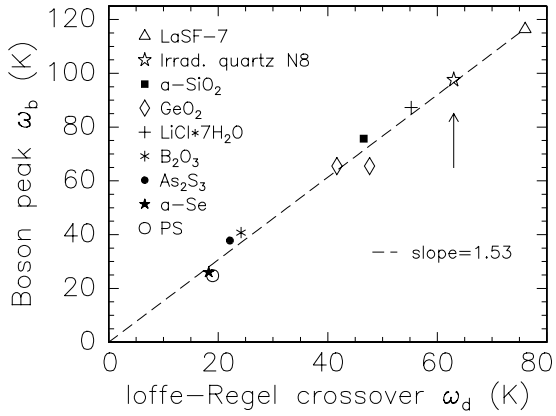

Fig. 7. Positions of the boson peak ω_b for different amorphous solids (from Raman spectra) versus Ioffe-Regel crossover frequency ω_d (from Ref. [25]). The arrow indicates the additional point for our sample N8.

the completely amorphized sample K17. Indeed, the temperature of the maximum in the low temperature velocity, which is an indication for the mean γ, is very similar in N6 and K17. This indicates a similar density of two-level systems in N6 and K17. Since according to the soft potential model the concentration of two-level systems and quasilocal harmonic oscillators are in a direct relation with each other, this also indicates that there might be nearly the same concentration of quasilocal harmonic oscillators in the crystalline part of N6 and in its amorphous part and in the completely amorphized sample K17.

We also measured the Raman spectrum in an irradiated vitreous silica sample K18-G, which is again another phase of a-SiO_2, for comparison. Vitreous silica after neutron irradiation with high dose ($\sim 1 \times 10^{20}$ n/cm^2) evolves to a similar metamict phase as neutron-irradiated quartz. Many authors consider it to be the same phase as the metamict phase, because many physical properties are the same within experimental error. This was observed in small-angle X-ray scattering and in Raman and infrared spectroscopy [40]. Mass density measurements also confirm these observations (see Fig. 1). Ultrasound measurements performed in our laboratory have indeed found the similar values of the macroscopic tunnelling parameter in the neutron-irradiated vitreous silica sample K18-G as in the irradiated quartz sample K17-Q (see Tab. 2) and it was found that the tunnelling density of states $\bar{P}$ is also quite similar.

In Table 2 we collected the parameters C_l and the boson peak frequencies ω_b of neutron-irradiated quartz and vitreous silica samples. One can see that the average value of $\bar{C}_l$ is nearly equal for all investigated samples and therefore, the calculated boson peak frequency is also equal. This is in very good agreement with the experimental observations. As can be seen from the last two columns of Table 2 the experimental values for the boson peak frequency ω_b agree very well with the values calculated from the equation (8). We should stress that no fitting parameters were used in our calculations. This is a surprising result for us since we expected to find a rather strong influence of the dose on ω_b since the structure of the irradiated quartz samples evolves from a 35% amorphous fraction to 100% and the mass density from 2.57 to 2.26 g/cm^3.

The obtained results strongly support the idea that the boson peak in irradiated quartz corresponds to the Ioffe-Regel criterion for acoustic phonons, established earlier for many amorphous solids. To illustrate this we show in Figure 7 (Ref. [25]) how the position of the boson peak in neutron-irradiated quartz fits exactly the theoretical predictions given by equation (8).

The observed behaviour of the boson peak in neutron-irradiated quartz and vitreous silica are very similar to that reported for the densified vitreous silica [55,56]. As one can see from the Table 2, the peak position in irradiated vitreous silica is shifted for 15 cm^{-1} to higher frequencies. A similar shift was observed in Raman spectra of permanently densified silica samples [55]. It was shown that this shift increases with increasing pressure used for the densification, and for the pressure of 16 GPa its value is also 15 cm^{-1}. Bates et al. [40] have also observed a similar shift (13 cm^{-1}) of the low-frequency peak in the Raman spectrum of irradiated a-SiO_2 (dose 2×10^{20} n/cm^2). It was concluded that as a result of irradiation, regions of more compacted structure are formed. The interaction between the soft oscillators inside such a region is stronger and therefore, according to the soft potential model, this leads to the shift of the boson peak to higher frequencies [24]. This result is also consistent with the conclusion of the inelastic neutron scattering study of densified silica samples [56] that the origin of the boson peak can be attributed to a soft mode, which is associated with the additional degree of freedom provided by the void space of the intermediate range structure. In the next section we will discuss the microscopic origin of the boson peak.

5 Origin of the boson peak in neutron-irradiated quartz and a-SiO_2

Lattice vibrations in α-quartz were intensively studied using Raman scattering [47,57–61], infrared [62], and

neutron scattering measurements [63]. Several theoretical models were proposed to explain the lattice dynamics of quartz [63–67]. At 573 °C quartz undergoes a phase transition from α phase with mass-density 2.65 g/cm^3 to the high-temperature β phase with mass-density 2.53 g/cm^3. β-quartz also has nine atoms per elementary cell, however its symmetry changes from trigonal D_3 to hexagonal D_6. Raman spectra of β-quartz were studied by Bates and Quist [68]. At 559 °C they observed a broad band with symmetry A_1 centered at 69 cm^{-1} that shifts to lower frequencies with increasing temperature and disappears under the Rayleigh wing above 580 °C. It was concluded that this band is connected with the phase transition.

It is known that in the case of a second-order phase transition in crystals, there occurs either a displacement of the sublattices of the crystal in the direction of one of the normal oscillations, or an ordering of the positions of the sublattices in accordance with certain oscillations. Ginzburg has developed the theory [69–71] which relates displacement type second-order phase transitions with the crystal lattice dynamics. According to this theory a soft mode should be a general characteristic of second-order phase transitions in all crystals. For the case of the $\alpha - \beta$ transition in quartz it was concluded that the frequency of at least one of the A_1 lines (207, 356, 1082 cm^{-1}) should become zero at the transition point and the intensity of this line increases. The line at zero frequency is due to the second-order Raman scattering and it is not only rather strong near the transition point, but also present above it.

Kleinman and Spitzer [65] have calculated the atomic motions and frequencies of the eight nondegenerate optical vibrations of α-quartz on the basis of a valence force model. They have shown that the 207 cm^{-1} vibration involves atomic motions very similar to those of the $\alpha - \beta$ transition. According to their work this mode is described as a motion of O atoms normal to the plane of the Si-O-Si unit. Their calculations revealed also that the O bending constant should be small and possibly negative.

Detailed Raman studies of the α–β transition [72] have indeed shown that a soft optic phonon at 207 cm^{-1} goes to zero frequency at the transition temperature. Moreover, it was proposed that this soft mode has a strong interaction with two zone-edge acoustic phonons, which are responsible for the A_1 Raman line at 147 cm^{-1} in $\alpha-$quartz. In a more recent study of β-quartz by means of hyper-Raman scattering [73], a silent soft phonon mode with symmetry B_1 at zero frequency was observed for the first time. This result validates the conclusion, that the α–β phase transition is a simple displacement type phase transition.

The transition mechanism was proposed in the model of Grimm and Dorner [74]. According to this model the SiO_4 tetrahedra are assumed to be rigid. During the α–β transition they rotate along their binary axis. The Si-atoms remain fixed to a first approximation. Rotations of tetrahedra are coupled along the chains. Thus the complete motion of the structure during the α–β transition is described by means of a single parameter: the tilt angle around the binary axis. This angle is about 7° at the transition temperature and a corresponding distance between the two possible oxygen sites is 0.3–0.4 Å.

Studies of the transition region using electron microscopy and neutron scattering [75–77] revealed the existence of the incommensurate phase within a small temperature interval of about 1.3 K between the usual α- and β-phases. It was observed that in the vicinity of the transition the α-phase breaks up into arrays of columnar triangular domains parallel with the c-axis. They have a Dauphiné twin structure, i.e. related by a 180° rotation around the c-axis, and are arranged following regular (hexagonal) networks. The size of the domains is about a few tens of nm, which decreases with increasing temperature. The domain walls (Dauphiné twin boundaries) are constantly vibrating, thus transforming continuously the $\alpha 1$ orientation into $\alpha 2$. From the observations of the particular geometry of the diffuse intensity observed in the electron diffraction patterns it was concluded that this geometry is related to the phonon mode, which drives the transition from α to β-phase. This diffuse scattering increases in intensity with temperature and it is present as well in the α as in the β-quartz. It is especially intense in the vicinity of the transition, but it still exists in the β-phase. Moreover, it is not related to the domain structure. It is present, within a single domain of the α-modification, as well as in the β-phase.

The analysis of the irradiation-induced structural changes in α-quartz using Raman [49,78,79] and X-ray spectroscopy [42,80] have shown that they are very similar to those observed during the α–β transition. The irradiation with fast neutrons produces not only amorphous regions with a size of about 20–30 Å, but also leads to the development of an increasing volume fraction of microtwins in the crystalline part of the irradiated samples. It turned out that the geometric model proposed by Grimm and Dorner [74] to explain the structural changes in quartz at α–β transition can be used for the calculation of the atomic positions for neutron-irradiated quartz [80]. X-ray spectroscopy has also shown that at a dose similar to that of our sample N6 the microtwin formation saturates and the lattice becomes hexagonal [42].

Ultrasound measurements performed in our laboratory have also led to the conclusion that the two-level systems created in neutron-irradiated quartz can be attributed to a rotational motion of the chains of tetrahedra, similar to those observed during the α–β transition [38,44]. This microscopic picture is similar to the model proposed by Buchenau et al. [4,5] for the vibrational modes observed by inelastic neutron scattering in vitreous silica (see Sect. 1).

Theoretical models for the irradiation-induced amorphization [81–83] show that during ion (and also fast neutron) irradiation there are clusters with liquid-like properties, which exist a very short time (10^{-12} s). We propose that the ultrafast cooling (10^{15} K/s) leads to the appearance of microdomains, which are frozen in in the crystalline environment (firstly inside these amorphous clusters and secondly in the crystalline matrix itself). Their existence we can see from the Raman spectra of our

irradiated quartz sample N6, which has a 65% crystalline fraction, from anisotropy in ultrasound velocity change and absorption (see Fig. 6). We can say that the fast neutron irradiation leads to the appearance of an agglomerative structure: separate amorphous clusters inside crystalline regions or for high doses inside amorphous regions. It is possible that such structure can exist also in high temperature polymorphs: tridymite and cristobalite. We propose that the same process occurs during glass formation: the formation of amorphous silica from the melt. This process is slower (10^5–10^{10} K/s). However, it is rather fast and a metastable microdomain structure appears in amorphous SiO_2 (frozen metastable phase transition structure). Therefore, the origin of the boson peak can be attributed to the soft optic mode that is characteristic for the α–β transition in quartz. This mode corresponds to the coupled libration motion of the tetrahedra along the chain as was described above and has a small restoring force. The same conclusion has been made in a recent inelastic neutron scattering experiment [12]. Hyper-Raman measurements of the boson peak in a-SiO_2 [6] have also shown that the intensity of the peak is very high. This high intensity of the second-order Raman scattering is characteristic for the α–β transition in quartz. The main differences between irradiation-induced amorphization and quenching amorphization can be the density and the size of these microdomains, and also the strength of the interaction between the local soft modes. Therefore, the position of the boson peak is different in amorphous silica and in highly irradiated quartz and a-SiO_2 samples.

6 Conclusions

We have verified the physical mechanism, which is proposed by the soft potential model to explain the appearance of the boson peak in low-frequency Raman spectra of amorphous and disordered solids. Comparing the experimental data on Raman scattering and the tunnelling parameters obtained from the ultrasound measurements in the same samples with the predictions of the soft potential model, our study confirms that the boson peak position in neutron-irradiated quartz crystals and amorphous silica corresponds to the Ioffe-Regel crossover frequency for acoustical phonons. The observed shape of the boson peak can also be explained in the framework of this model, which assumes that the quasilocal optic-like vibrations provide the main contribution to this peak.

However, our study cannot answer on the question concerning the frequency dependence of the Raman coupling constant. It would be very useful from our point of view to measure hyper-Raman spectra in the same samples, because as was observed in vitreous silica, the vibration modes which are not active in Raman scattering contribute substantially in the boson peak observed in hyper-Raman scattering [6].

Our observation of the boson peak in sample N6 with the lowest dose (4.7×10^{19} n/cm^2) that is mainly crystalline shows that this dose is sufficient to create the concentration of quasilocal vibrations, which is necessary for the appearance of this peak. Moreover, these vibration modes reside not only in amorphous clusters created by fast neutrons, but also in the disturbed crystalline part of the sample. This observation supports the results of the previous low-temperature ultrasound measurements, which have shown the high concentration of the tunnelling states in the crystalline part of the sample. It confirms the idea about the common origin of the tunnelling states and quasilocal vibrations in neutron-irradiated quartz and also in vitreous silica.

From the detailed analysis of the Raman and X-ray scattering, and also electron microscopy data of quartz during α–β transition and the results of our Raman scattering and the previous low-temperature ultrasound measurements in neutron-irradiated quartz, we have put forward a model for the origin of the boson peak in neutron-irradiated quartz and vitreous silica. This origin is the soft optic-like mode analogous to the soft mode that drives the α–β transition in quartz. This mode corresponds to the coupled libration motion of the tetrahedra along the chain and is responsible for the appearance of the microdomain structure during the phase transition. Such microdomains are created by fast neutrons in quartz crystals or during the quenching from the melt in vitreous silica. The interaction between the local optic modes is mediated by acoustic phonons. The position of the peak depends on the concentration and size of these modes and also on the strength of their interaction.

References

1. R.H. Stolen, Phys. Chem. Glass. **11**, 83 (1970)
2. R. Shuker, R.W. Gammon, Phys. Rev. Lett. **25**, 222 (1970)
3. A.J. Martin, W. Brenig, Phys. Stat. Sol. **64**, 163 (1974)
4. U. Buchenau, N. Nücker, A.J. Dianoux, Phys. Rev. Lett. **53**, 2316 (1984)
5. U. Buchenau, M. Prager, N. Nücker, A.J. Dianoux, N. Ahmad, W.A. Phillips, Phys. Rev. B **34**, 5665 (1986).
6. B. Hehlen, E. Courtens, R. Vacher, A. Yamanaka, M. Kataoka, K. Inoue Phys. Rev. Lett. **84**, 5355 (2000)
7. P. Benassi, M. Krisch, C. Masciovecchio, V. Mazzacurati, G. Monaco, G. Ruocco, F. Sette, R. Verbeni, Phys. Rev. Lett. **77**, 3835 (1996)
8. O. Pilla, A. Consulo, A. Fontana, C. Masciovecchio, G. Monaco, M. Montagna, G. Ruocco, T. Scopigno, F. Sette, Phys. Rev. Lett. **85**, 2136 (2000)
9. E. Courtens, M. Foret, B. Hehlen, R. Vacher, Solid State Commun. **117**, 187 (2001)
10. B. Rufflé, M. Foret, E. Courtens, R. Vacher, G. Monaco, Phys. Rev. Lett. **90**, 095502 (2003)
11. E. Courtens, M. Foret, B. Hehlen, B. Rufflé, R. Vacher, J. Phys.: Condens. Matter **15**, 1279 (2003)
12. A. Wischnewski, U. Buchenau, A.J. Dianoux, W.A. Kamitakahara, J.L. Zarestky, Philos. Mag. B **77**, 579 (1998)
13. V.G. Karpov, M.I. Klinger, F.N. Ignatiev, Sov. Phys. JETP **57**, 439 (1983)
14. M.A. Il'in, V.G. Karpov, D.A. Parshin, Sov. Phys. JETP **65**, 165 (1987)
15. U. Buchenau, Yu.M. Galperin, V.L. Gurevich, H.R. Schober, Phys. Rev. B **43**, 5039 (1991)

16. U. Buchenau, Yu.M. Galperin, V.L. Gurevich, D.A. Parshin, M.A. Ramos, H.R. Schober, Phys. Rev. B **46**, 2798 (1992)
17. M.A. Ramos, U. Buchenau, Phys. Rev. B **55**, 5749 (1997)
18. E.R. Grannan, M. Randeria, J.P. Sethna, Phys. Rev. Lett. **60**, 1402 (1988)
19. M. Randeria, J.P. Sethna, Phys. Rev. B **38**, 12607 (1988)
20. E.R. Grannan, M. Randeria, J.P. Sethna, Phys. Rev. B **41**, 7784 (1990)
21. E.R. Grannan, M. Randeria, J.P. Sethna, Phys. Rev. B **41**, 7799 (1990)
22. J.P. Sethna, E.R. Grannan, M. Randeria, Physica B **169**, 316 (1991)
23. V.L. Gurevich, D.A. Parshin, J. Pelous, H.R. Schober, Phys. Rev. B **48**, 16318 (1993)
24. V.L. Gurevich, D.A. Parshin, H.R. Schober, Phys. Rev. B **67**, 094203 (2003)
25. D.A. Parshin, C. Laermans, Phys. Rev. B **63**, 132203 (2001)
26. S.R. Elliott, Europhys. Lett. **19**, 201 (1992)
27. L. Börjesson, A.K. Hassan, J. Swenson, L.M. Torell, A. Fontana Phys. Rev. Lett. **70**, 1275 (1993)
28. A.P. Sokolov, R. Calemczuk, B. Salce, A. Kisliuk, D. Quitmann, E. Duval, Phys. Rev. Lett. **78**, 2405 (1997)
29. W. Schirmacher, G. Diezemann, C. Ganter, Phys. Rev. Lett. **81**, 136 (1998)
30. J.W. Kantelhardt, S. Russ, A. Bunde, Phys. Rev. B **63**, 064302 (2001)
31. S.N. Taraskin, Y.L. Loh, G. Natarajan, S.R. Elliott, Phys. Rev. Lett. **86**, 1255 (2001)
32. W. Götze, M.R. Mayr, Phys. Rev. E **61**, 587 (2000)
33. T. Nakayama, Rep. Prog. Phys. **65**, 1195 (2002)
34. T.S. Grigera, V. Martin-Mayor, G. Parisi, P. Verrocchio, J. Phys.: Condens. Matter **14**, 2167 (2002)
35. C. Laermans, B. Daudin, in *Phonon Scattering in Condensed Matter*, edited by H. Maris (Plenum Press, 1980), p. 21
36. J.W. Gardner, A.C. Anderson, Phys. Rev. B **23**, 474 (1981)
37. A. Vanelstraete, C. Laermans, Phys. Rev. B **42**, 5842 (1990)
38. C. Laermans, V. Keppens, Phys. Rev. B **51**, 8158 (1995)
39. J. Classen, I. Rohr, C. Enss, S. Hunklinger, C. Laermans, Eur. Phys. J. B **10**, 623 (1999)
40. J.B. Bates, R.W. Hendricks, L.B. Shaffer, J. Chem. Phys. **61**, 4163 (1974)
41. F. Terki, C. Levelut, M. Boissier, J. Pelous, Phys. Rev. B **53**, 2411 (1996); the used neutron-irradiated quartz samples were those of our laboratory
42. R. Comes, M. Lambert, A. Guinier, in *Interaction of Radiation with Solids*, edited by A. Bishay (Plenum, New York, 1967), p. 319
43. A. Vanelstraete, Ph.D. thesis, Katholieke Universiteit Leuven, Belgium (1988)
44. V. Keppens, Ph.D. thesis, Katholieke Universiteit Leuven, Belgium (1995)
45. V. Keppens, C. Laermans, Phys. Rev. B **53**, 14849 (1996)
46. G. Winterling, Phys. Rev. B **12**, 2432 (1975)
47. J. F. Scoot, S.P.S. Porto, Phys. Rev. **161**, 903 (1967)
48. V.J. Tekippe, A.K. Ramdas, S. Rodriguez, Phys. Rev. B **8**, 706 (1973)
49. N. Elkhayati Elidrissi, Ph.D. thesis, Université des Sciences et Techniques du Languedoc, Montpellier, France (1986)
50. S. Hunklinger, A.K. Raychaudhuri, *Progress in Low Temperature Physics*, edited by D.F. Brewer (Elsevier, Amsterdam, 1986), Vol. IX, p. 265
51. W. Dietsche, H. Kinder, Phys. Rev. Lett. **43**, 1413 (1979)
52. D.P. Jones, N. Thomas, W.A. Phillips, Phil. Mag. B **38**, 271 (1978)
53. J.E. Graebner, B. Golding, L.C. Allen, Phys. Rev. B **34**, 5696 (1986)
54. V. Keppens, C. Laermans, Physica B, **263–264**, 149 (1999)
55. S. Sugai, A. Onodera, Phys. Rev. Lett. **77**, 4210 (1996)
56. Y. Inamura, M. Arai, M. Nakamura, T. Otomo, N. Kitamura, S.M. Bennington, A.C. Hannon, U. Buchenau, J. Non-Cryst. Solids **293–295**, 389 (2001)
57. R.S. Krishnan, Nature, Lond. **155**, 452 (1945)
58. P.K. Narayanaswamy, Proc. Indian Acad. Sci. **26A**, 521 (1947)
59. D. Krishnamurti, Proc. Indian Acad. Sci. **47A**, 276 (1958)
60. V.G. Zubov, L.P. Osipova, Kristallografiya **6**, 418 (1961); V.G. Zubov, L.P. Osipova, Sov. Phys. Crystallography **6**, 330 (1961)
61. D.F. Kiselev, L.P. Osipova, Kristallografiya **11**, 279, 401 (1966); D.F. Kiselev, L.P. Osipova, Sov. Phys. Crystallography **11**, 255, 000 (1966)
62. W.G. Spitzer, D.A. Kleinman, Phys. Rev. **121**, 1324 (1961)
63. M.M. Elcombe, Proc. Phys. Soc. **91**, 947 (1967)
64. B.D. Saksena, H. Narain, Proc. Ind. Acad. Sci. **A30**, 128 (1949)
65. D.A. Kleinman, W.G. Spitzer, Phys. Rev. **125**, 16 (1962)
66. M.E. Stiefler, G.R. Barsch, Phys. Rev. B **12**, 4553 (1975)
67. T.H.K. Barron, C.C. Huang, A. Pasternak, J. Phys. C **9**, 3925 (1976)
68. J.B. Bates, A.S. Quist, J. Chem. Phys. **56**, 1528 (1972)
69. V.L. Ginzburg, Fiz. Tverd. Tela **2**, 2031 (1960); V.L. Ginzburg, Soviet Phys., Solid State **2**, 1824 (1961)
70. V.L. Ginzburg, A.P. Levanyuk, Zh. Eksp. Teor. Fiz. **39**, 192 (1960); V.L. Ginzburg, A.P. Levanyuk, Soviet Phys., JETP **12**, 138 (1961)
71. V.L. Ginzburg, Usp. Fiz. Nauk **77**, 621 (1962); V.L. Ginzburg, Soviet Phys. Usp. **5**, 649 (1963)
72. J.F. Scott, Phys. Rev. B **21**, 907 (1968)
73. Y. Tezuka, S. Shin, M. Ishigame Phys. Rev. Lett. **66**, 2356 (1991)
74. H. Grimm, B. Dorner, J. Phys. Chem. Solids **36**, 407 (1975)
75. G. Van Tendeloo, J. Van Landuyt, S. Amelinckx, Phys. Stat. Sol. (a) **30**, K11 (1975)
76. G. Van Tendeloo, J. Van Landuyt, S. Amelinckx, Phys. Stat. Sol. (a) **33**, 723 (1976)
77. G. Dolino, J.P. Bachheimer, B. Berge, C.M.E. Zeyen, G. Van Tendeloo, J. Van Landuyt, S. Amelinckx, J. Phys. France **45**, 901 (1984)
78. V.G. Zubov, L.P. Osipova, Krystallografiya **15**, 992 (1970)
79. V.G. Zubov, L.P. Osipova, Krystallografiya **22**, 110 (1977); V.G. Zubov, L.P. Osipova, Soviet Phys. Crystallography **22**, 61 (1977)
80. E.V. Kolontsova, A.E. Korneev, V.P. Lutsenko, Dokl. Akad. Nauk SSSR **247**, 80 (1979); E.V. Kolontsova, A.E. Korneev, V.P. Lutsenko, Sov. Phys. Dokl. **24**, 556 (1979)
81. L.A. Bursil, G. Braunshausen, Philos. Mag. A **62**, 395 (1990)
82. G. Szenes, Phys. Rev. B **52**, 6154 (1995)
83. S.X. Wang, L.M. Wang, R.C. Ewing, R.H. Doremus, J. Non-Cryst. Solids **238**, 198 (1998)